nature chemistry

ARTICLES

PUBLISHED ONLINE: 13 JUNE 2016 | DOI: 10.1038/NCHEM.2535

Accurate first-principles structures and energies of diversely bonded systems from an efficient density functional

Jianwei Sun[1]*, Richard C. Remsing[2,3], Yubo Zhang[1], Zhaoru Sun[1], Adrienn Ruzsinszky[1], Haowei Peng[1], Zenghui Yang[1], Arpita Paul[4], Umesh Waghmare[4], Xifan Wu[1], Michael L. Klein[1,2,3] and John P. Perdew[1,2]

One atom or molecule binds to another through various types of bond, the strengths of which range from several meV to several eV. Although some computational methods can provide accurate descriptions of all bond types, those methods are not efficient enough for many studies (for example, large systems, *ab initio* molecular dynamics and high-throughput searches for functional materials). Here, we show that the recently developed non-empirical strongly constrained and appropriately normed (SCAN) meta-generalized gradient approximation (meta-GGA) within the density functional theory framework predicts accurate geometries and energies of diversely bonded molecules and materials (including covalent, metallic, ionic, hydrogen and van der Waals bonds). This represents a significant improvement at comparable efficiency over its predecessors, the GGAs that currently dominate materials computation. Often, SCAN matches or improves on the accuracy of a computationally expensive hybrid functional, at almost-GGA cost. SCAN is therefore expected to have a broad impact on chemistry and materials science.

Kohn–Sham density functional theory (DFT) is the most widely used electronic structure method because of its computational efficiency and reasonable accuracy. It delivers the exact ground-state total energy and electron density, derived from theory, while its exchange-correlation energy E_{xc}, the 'glue' that binds one atom to another, must be approximated in practice. The local density approximation (LDA)[1–3], the first approximation in DFT, constructs a local energy density at position $\mathbf{r}$ from just the local electron density $n(\mathbf{r}) = \sum_i^{occ} |\varphi_i|^2$, where φ_i are occupied Kohn–Sham orbitals (spin is suppressed here).

The LDA was derived from (and is exact for) any uniform electron gas[1], and tends to minimize the inhomogeneity of the electron densities of real materials and overestimate the strengths of all bonds near equilibrium. By introducing the electron density gradient to reduce this tendency, generalized gradient approximations (GGAs) soften bonds. Depending on how the electron density gradient is built in[4,5], a GGA can be rather accurate for structures or energies, but not for both[6]. This dilemma probably reflects a formal limitation: a GGA cannot satisfy all the known exact constraints appropriate to a semilocal functional (LDA, GGAs and meta-GGAs) where the exchange-correlation energy is efficiently evaluated as a single integral over three-dimensional space. For example, it is impossible for a GGA to simultaneously satisfy the slowly varying density limit[1] for extended systems and the tight lower bound on the exact exchange energy of single-orbital systems[7] while still delivering accurate exchange energies[8]. Semilocal functionals can be accurate for electron densities for which the exchange-correlation hole around an electron is sufficiently localized. Therefore, exact constraints consistent with this condition are appropriate to semilocal functionals. Among GGAs, the standard Perdew–Burke–Ernzerhof (PBE) GGA[4] gives balanced descriptions for structures and energies with a significant overall improvement over LDA. However, the non-empirical PBE GGA largely loses the intermediate-range van der Waals interaction, the strength of which is overestimated in the LDA.

Introducing the kinetic energy density $\tau = (1/2)\sum_i^{occ} |\nabla\varphi_i|^2$ within meta-GGAs[8–15] is a way to circumvent this 'structure or energy' dilemma. Because the occupied orbitals are already there for constructing the non-interacting kinetic energy, their use to construct the exchange-correlation energy semilocally adds little to the computational cost. The kinetic energy density for a uniform electron gas is $\tau^{unif} = (3/10)(3\pi^2)^{2/3}n^{5/3}$, and $\tau^w = (1/8)|\nabla n|^2/n$ for the single-orbital systems. By using the dimensionless variable $\alpha = (\tau - \tau^w)/\tau^{unif}$, meta-GGAs can recognize the slowly varying densities ($\alpha \sim 1$, characterizing metallic bonds) and single-orbital systems ($\alpha = 0$, characterizing covalent single bonds) and thus reduce to different GGAs for these two dramatically different limits[8,13,15]. α also has the power to identify non-covalent bonds with $\alpha \gg 1$ between two closed shells, where τ from the anti-bonding[16] highest-occupied molecular orbital overwhelms τ^{unif} and τ^w. α is directly related to the electron localization function (ELF)[17], where $ELF = 1/(1+\alpha^2)$, and therefore identifies different chemical bonds[18,19]. Other dimensionless variables built from τ have been used by meta-GGAs (for example, by the Tao–Perdew–Staroverov–Scuseria (TPSS)[10] and M06L[11] meta-GGAs). However, due to the inability of these dimensionless variables to distinguish among different chemical bonds, TPSS largely misses the van der Waals interaction and M06L shows strong numerical instability for single bonds[19].

The strongly constrained and appropriately normed (SCAN) meta-GGA[15] takes advantage of the above flexibility to satisfy all 17 exact constraints appropriate to a semilocal functional, including the tight lower bound[7] on the exchange energy. It then uses

[1]Department of Physics, Temple University, 1925 N 12th Street, Philadelphia, Pennsylvania 19122, USA. [2]Department of Chemistry, Temple University, 1901 N 13th Street, Philadelphia, Pennsylvania 19122, USA. [3]Institute for Computational Molecular Science, Temple University, 1925 N 12th Street, Philadelphia, Pennsylvania 19122, USA. [4]Theoretical Sciences Unit, Jawaharlal Nehru Centre for Advanced Scientific Research, Bangalore 560064, India. *e-mail: jianweisun791012@gmail.com

appropriate norms, where the exact exchange-correlation hole is sufficiently localized (for example, the hydrogen atom), as guidance across the constraints. Although SCAN uses no bonded information in its construction, the power of α together with the strong constraints and appropriate norms make it accurate for diversely bonded materials, with genuine non-empirical predictive power.

Due to the semilocal feature in the computation, meta-GGAs are much more efficient than hybrid GGAs, which are the current beyond-GGA choice. By mixing GGAs with non-local exact exchange, hybrid GGAs (for example, the PBE0 hybrid GGA[20], where 25% of the exact exchange energy is mixed with 75% of PBE GGA exchange) can further improve the description of covalent, ionic and hydrogen bonds. However, hybrid GGAs still fail to describe van der Waals interactions. PBE0 is especially hard to evaluate for metallic systems, although some range-separated versions (without long-range exact exchange) are easier. The computational cost of a hybrid functional can be 10 to 100 times[21] that of a semilocal functional in standard plane-wave codes. Another problem with hybrids is that a universal exact-exchange mixing parameter is not determined by any exact condition, nor is the range-separation parameter in a range-separated hybrid.

The SCAN meta-GGA has been shown[15] to be superior to the PBE GGA for some standard molecular test sets and a small collection of solids. The mean absolute errors for SCAN[15] are smaller than those for PBE by a factor of about 4 for the atomization energies of the 223 G3 molecules, a factor of 3 for the binding energies of the S22 set of weakly bound dimers of small molecules, and a factor of 4 for the LC20 set of lattice constants for solids. SCAN is also more accurate, by about 30%, in predicting the BH76 energy barriers to chemical reactions. Future studies will also show that the mean absolute errors of SCAN for the heats of formation of 94 binary solids are smaller than those of PBE by about 30%, or a factor of 3, for compounds with or without transition-metal elements, respectively. However, this Article shows that SCAN has an unexpected and striking performance for diversely bonded systems, many of which were believed to be out of reach of semilocal functionals, and is comparable to or even more accurate than a computationally more expensive hybrid GGA.

Results and discussion

Van der Waals interactions in ice phases and water hexamer clusters. It was once believed that non-empirical semilocal functionals and their hybrids were incapable of describing the van der Waals bonds arising from intermediate-range van der Waals interactions. Van der Waals interactions are typically weak, but still important (for example, for the structures of a hydrogen-bonded network like ice). In the binding energy difference per H_2O between one ice phase and another, the van der Waals attraction becomes more important compared with the hydrogen-bonding energies when the density of water molecules increases[22]. Figure 1a shows that both the PBE GGA and PBE0 hybrid significantly destabilize high-pressure phases relative to Ih (the stable phase of ice at ambient pressure), and the addition of the Tkatchenko–Scheffler[23] van der Waals correction (vdW_TS) improves the energy differences dramatically compared to the experimental results or the highly accurate yet expensive diffusion Monte Carlo (DMC) predictions[22,24]. Interestingly, and surprisingly, the SCAN meta-GGA[15] yields energy differences between all the different ice phases studied here with an accuracy comparable to that of PBE0+vdW_TS and considerably improves upon the predictions of PBE0+vdW_TS for the energy difference between ice Ih and the high-density phase VIII. Moreover, SCAN predicts that ice II is 3 meV per H_2O more stable than ice IX, in agreement with experiments, while this ordering is reversed by both PBE+vdW_TS and PBE0+vdW_TS. This might be due to the many-body nature of the van der Waals interaction, which is missed by the pairwise vdW_TS correction but captured by SCAN. The lower panel of Fig. 1a also shows that SCAN predicts the volume changes between ice phases in near-quantitative agreement with the experimental results and thus with greater accuracy than all other functionals considered here.

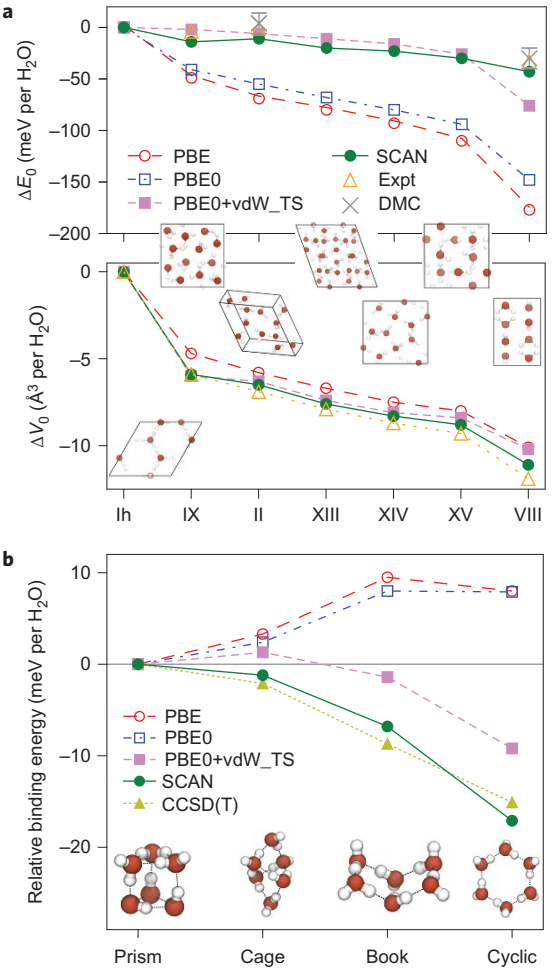

Figure 1 | SCAN captures the intermediate-range, many-body van der Waals interactions necessary for a quantitative description of various ices and gas-phase water hexamers. a, The relative sublimation energy ΔE_0 and equilibrium volume change ΔV_0 per water molecule of seven hydrogen-ordered ice phases with respect to the ground-state ice Ih illustrate that SCAN is the only functional tested that predicts the relative stability of ice phases in quantitative agreement with experimental results. The sublimation energy (E_0) is the energy needed to break an ice into isolated water molecules. **b**, The relative binding energy per water molecule of four low-energy water hexamers similarly illustrates that SCAN is the only semi-local density functional approximation that predicts the known energetic ordering of these clusters, evidenced by the agreement between SCAN and CCSD(T). The zero-point energy effects have been removed from the experimental results[46,47] for ice. Data points (and error bars) computed by methods other than SCAN are from refs 24 and 25 for the ice phases and water hexamers, respectively. Lines are guides to the eye.

In addition to ice in its different phases, water clusters also present a challenge for semilocal and hybrid density functionals. Water hexamer clusters are the most notorious examples[25]. The water hexamer has four low-energy configurations: prism, cage, book and cyclic. High-level wavefunction methods[25] (for example, the coupled cluster singles and doubles with perturbative triples, CCSD(T)) all predict the prism configuration to be the most stable, followed by the cage, book and cyclic structures. However,

Table 1 | Properties of the water monomer, dimer, hexamer (at the prism configuration) and ice Ih at equilibrium.

	LDA	PBE	PBE0	PBE+vdW_TS	PBE0+vdW_TS	SCAN	Best *ab initio*	Expt
R(O–H)	0.970	0.970	0.959	0.969	0.957	0.961	–	0.957
∠HOH	105.0	104.2	104.9	104.2	104.9	104.4	–	104.5
ν_1	3,837	3,802	3,962	3,810	–	3,911	–	3,943
ν_2	3,726	3,697	3,857	3,706	–	3,806	–	3,832
ν_3	1,551	1,592	1,633	1,595	–	1,647	–	1,648
μ	1.858	1.804	1.854	1.804	1.853	1.847	–	1.855
α	10.24	10.33	9.58	–	–	9.81	9.65	9.63 ± 0.20
β	36.0	35.5	28.7	–	–	34.4	29.6	–
R(O–O)	2.71	2.90	2.89	2.90	2.89	2.86	2.91	2.98
E_b^D	193.6	109.7	106.7	117.8	113.7	118.3	108.8	108 ± 1
E_b^H	–	336.1	322.9	369.6	360.6	376.8	347.6	–
V_0	25.37	30.79	30.98	29.67	29.88	29.56	31.69 ± 0.01	30.91
E_0	1095	636	598	714	672	660	605 ± 5	610

For the water monomer, R(O–H) is the bond length (Å); ∠HOH is the bond angle; ν_1, ν_2 and ν_3 are the vibrational frequencies (cm^{-1}) (ν_1 and ν_2 are the asymmetric and symmetric O–H stretching modes and ν_3 is the H–O–H bending mode); μ is the dipole moment (Debye); α is the isotropic polarizability; and β is the magnitude of the hyperpolarizability. α and β are in atomic units. For the water dimer, R(O–O) is the distance between the two oxygen atoms and E_b^D is the binding energy (meV per H_2O). E_b^H is the binding energy (meV per H_2O) for the hexamer. The last two rows show the volume V_0 (Å) and sublimation energy E_0 (meV per H_2O) of ice Ih at equilibrium. The experimental values and the best *ab initio* estimations for the water monomer and dimer are from ref. 48. The experimental E_b^D is estimated by subtracting the DMC zero-point vibrational energy[49] from the experimentally measured dissociation energy[50]. The best *ab initio* estimates of α and β are the CCSD(T) values from ref. 51 and that of the hexamer is the CCSD (T) value from ref. 25. For ice Ih, the zero-point energy effects have been extracted in the experimental results[46,47] and values other than LDA and SCAN are from refs 24 and 25.

PBE and PBE0 predict prism to be the most unstable and book the most stable. Adding the vdW_TS stabilizes prism more than book and cyclic, but cage is still more favoured than prism. Strikingly, again, SCAN predicts the correct energetic ordering of the hexamers and quantitatively follows the CCSD(T) results, as shown in Fig. 1b.

The accurate SCAN description of the ice polymorphs and water hexamers defies the conventional wisdom and shows that SCAN has the ability to capture the intermediate-range van der Waals interaction[11,19]. Of course, SCAN cannot describe the long-range van der Waals interaction, which exists even for non-overlapping electron densities.

Covalent and hydrogen bonding in water monomer, dimer, hexamer and ice Ih. In H_2O, the hydrogen atoms and oxygen atom are covalently bonded with an angle of about 105° between the OH bonds. An accurate description of these covalent bonds is of paramount importance to modelling water from first principles, because the resultant molecular structure underlies its hydrogen-bonding network. All the functionals considered in Table 1 give reasonably accurate predictions for the bond length and bond angle as well as the vibrational frequencies and dipole moment of a single water molecule, while PBE0 and SCAN are the best among them in comparison with the experimental results, demonstrating that SCAN is highly accurate for covalent bonds. Despite the reasonable description of the monomer provided by these functionals, their accuracy in describing hydrogen bonds varies. LDA is seldom used for the study of water due to its overestimation of the strengths of the hydrogen bonds, as supported by the data in Table 1. PBE greatly improves the binding energies of the water dimer, hexamer (at the prism configuration) and ice Ih. After including the missing van der Waals interaction, PBE+vdW_TS slightly overestimates the binding energies, suggesting that PBE overestimates the strength of the hydrogen bonds. SCAN, capturing the intermediate-range van der Waals interaction as demonstrated above, performs similarly to PBE+vdW_TS for the binding energies and thus also overestimates the strength of the hydrogen bonds. Indeed, pair correlations between the oxygen nuclei and centres of maximally localized Wannier functions, essentially representing lone pairs, are similar in SCAN and PBE (see Supplementary Information), quantitatively supporting this conclusion[26]. Semilocal functionals usually overestimate the polarizability and hyperpolarizability of the water molecule, as shown in Table 1, which can lead to a too large dipole moment for a water molecule bound to other water molecules[26] and thus to an overestimated hydrogen bond. Overestimated polarizabilities and hyperpolarizabilities are typically improved by exact-exchange mixing or self-interaction correction[27,28], as demonstrated in Table 1 by PBE0. This improvement is also manifested in the binding energies from PBE+vdW_TS to PBE0+vdW_TS.

Covalent and metallic bonding in crystalline and liquid Si. Silicon crystallizes under ambient conditions in the diamond structure with a coordination number of 4 and undergoes a semiconductor–metal phase transition at around 12 GPa of pressure into the β-Sn structure with a coordination number of 6. Figure 2a shows that, compared to experiment or to computationally expensive high-level DMC calculations[29], both LDA and PBE give accurate volumes for Si in the diamond and β-Sn phases, but PBE gives a more realistic yet still unsatisfactory energy difference between them. On the other hand, SCAN and the Heyd–Scuseria–Ernzerhof (HSE) hybrid GGA[30], a range-separated version of the PBE0 hybrid GGA, predict the energy difference of the two phases in excellent agreement with the DMC result.

It has been argued[29] that semilocal functionals do not predict an accurate energy difference between these two phases because they significantly underestimate the bandgap of the diamond phase, while HSE improves the bandgap and therefore the energy difference. However, this is not a satisfactory explanation. SCAN gives a bandgap of diamond Si only about halfway between PBE and experiment, but a very accurate structural energy difference. The improvement in the energy difference comes from the ability of SCAN to distinguish between covalent and metallic bonds and to properly stabilize covalent single bonds[31].

Figure 2b shows that SCAN significantly improves the interstitial defect formation energies of diamond Si when compared with LDA and PBE, reaching the level of accuracy of the HSE hybrid. The three lowest-energy interstitial defects in Si are T (tetrahedral site), H (hexagonal) and X (split), for which DMC predicts defect formation energies of 5.05, 5.13 and 4.94 eV, respectively[32]. However, these DMC values were calculated using GGA-relaxed geometric structures in a small supercell. The best interstitial formation energies estimated from experiments[29] are in the range of 4.23–4.85 eV, with which the results of both SCAN and HSE are in excellent agreement.

On melting, Si undergoes a transition from a semiconducting solid to a metallic liquid that contains transient covalent bonds between neighbouring atoms. The properties of liquid Si (*l*-Si) depend sensitively on the relative amounts of metallic and covalent bonding present in solution, and we find that SCAN provides a good description of this complex liquid. Simulations of *l*-Si in the

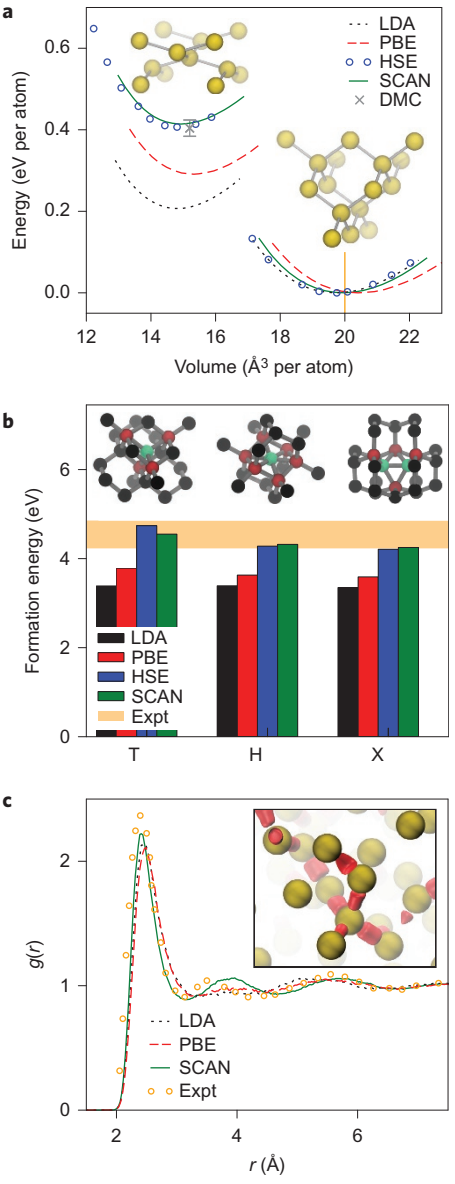

Figure 2 | SCAN simultaneously describes covalent and metallic bonding across the Si phase diagram. a, The energy difference between the metallic β-Sn (left inset) and semiconducting diamond (right inset) phases of Si is quantitatively captured by SCAN, as evidenced by the agreement with hybrid functional (HSE) and diffusion Monte Carlo (DMC) results. The vertical line indicates the experimental volume[29] of diamond Si. The error bar on the DMC result includes finite-size error estimates and statistical errors[32]. **b**, The interstitial defect formation energy in diamond Si is also quantitatively captured by SCAN. The SCAN predictions are within the range of the experimental results[29] (orange) for tetrahedral (T), hexagonal (H) and split (X) defects. Defect atoms are in green, their nearest neighbours in red and those in the second coordination shell in black. **c**, The pair correlation function $g(r)$ of liquid Si at $T = 1{,}800$ K involves a discrimination between metallic and covalent bonding in the liquid state. SCAN can describe this coexistence, resulting in better agreement with experimental results[34]. Inset: snapshot of liquid Si using SCAN highlights the existence of transient covalent bonding, with red isosurfaces of electron density corresponding to covalent bonds between tetrahedrally arranged Si atoms (yellow).

isothermal–isobaric ensemble at $T = 1{,}800$ K and $P = 0$ bar yield a density of 2.57 g cm^{-3} from SCAN, in good agreement with the experimental value[33] of 2.59 g cm^{-3}, whereas PBE (2.54 g cm^{-3}) slightly underestimates and LDA (2.70 g cm^{-3}) overestimates the density, as expected. SCAN also yields a position of the first peak of the pair correlation function $g(r)$ that is in excellent agreement with that of experiment[34], as shown in Fig. 2c, while those of LDA and PBE are shifted to slightly larger distances. The SCAN description of *l*-Si leads to a pronounced second peak in $g(r)$, as in the experimental results, albeit shifted to larger distances. Such a pronounced second peak is lacking in both LDA and PBE descriptions. The increased accuracy of SCAN with respect to PBE and LDA is again due to a better discrimination of metallic and covalent bonds, with the latter manifesting the tetrahedral coordination structure of molten Si, highlighted by the simulation snapshot showing an electron density corresponding to covalent bonds between Si atoms in a tetrahedral arrangement.

Ionic bonding in ferroelectric and multiferroic materials. Interactions between ionic species can be primarily electrostatic in origin, but can also have a significant component of van der Waals interactions among highly polarizable negative ions as well as covalent characteristics between nearest-neighbour ions[35], making the description of such systems challenging. SCAN has been shown to be remarkably good for describing solid MnO_2 (ref. 36). Here, SCAN was tested on two types of ionic material that are more stringent tests of density functionals. These are ferroelectric materials such as the prototypical $BaTiO_3$ and $PbTiO_3$, which exhibit spontaneous electric polarization due to structural instabilities at low temperature[37], and multiferroic materials like $BiFeO_3$, with ferroelectric and antiferromagnetic properties[38] (Table 2). The prediction of structural instabilities from first-principles calculations is extremely sensitive to volume changes, and even small errors of 1–2% in the lattice constants obtained from LDA and PBE yield unsatisfactory predictions for ferroelectric materials. PBE, for example, is particularly poor in its description of these materials, as it predicts spurious supertetragonality (too large c/a, where c/a is the ratio of lattice constants c and a) in $BaTiO_3$ and $PbTiO_3$ (ref. 37).

Efforts have been made to design functionals for solids to remedy this deficiency. The B1WC hybrid GGA[37] was designed for ferroelectric materials. It mixes 16% of exact exchange energy with 84% of Wu–Cohen (WC) GGA exchange[39] to fit the properties of $BaTiO_3$. Table 2 shows that B1WC predicts volumes for these three materials in excellent agreement with the experimental results, as well as very accurate c/a ratios and polarizations for $BaTiO_3$ and $PbTiO_3$. On the other hand, the more commonly used HSE hybrid GGA inherits the spurious supertetragonality for $BaTiO_3$ and $PbTiO_3$ from its parent PBE GGA[37] (although less severely) and predicts too large polarizations. SCAN is overall almost comparable to the computationally expensive B1WC and much better than LDA and PBE for the above properties. The SCAN energy differences between the cubic and tetragonal phases are much closer to the B1WC values than either LDA, PBE or even HSE.

SCAN also yields more realistic bandgaps for these compounds than LDA and PBE, consistent with our findings in Si and other semiconductors. This is possible because the SCAN meta-GGA, like the hybrid functionals, is implemented in a generalized Kohn–Sham scheme in which the exchange-correlation potential is not a multiplicative operator. Gaps of hybrid GGAs are, however, more realistic than SCAN gaps.

For the magnetic moment of Fe in $BiFeO_3$, PBE predicts the most accurate value (3.70 μB) in comparison with the experimental one (3.75 μB), while SCAN is the second best with 3.96 μB, and B1WC significantly overestimates this value. Remarkably, for ferroelectrics and multiferroics the non-empirical and semilocal SCAN meta-GGA is often comparable to or better than a hybrid functional fitted to $BaTiO_3$.

In studies of multiferroics, where late 3*d* transition metals are usually present to provide the magnetic properties, the Hubbard U

Table 2 | Properties of prototypical ferroelectric ($BaTiO_3$ and $PbTiO_3$) and multiferroic ($BiFeO_3$) materials predicted by LDA, PBE with and without the Hubbard U correction, SCAN and hybrid GGAs.

System	Property	LDA	PBE ($U = 2$)	HSE	SCAN	B1WC	Expt
$BaTiO_3$	E_g	1.72	1.73	3.27	2.13	3.44	3.38
	V_0	62.1	67.5	64.5	65.1	63.2	64.0
	c/a	1.011	1.054	1.039	1.029	1.015	1.010
	P_s	0.24	0.47	0.41	0.35	0.28	0.27
	ΔE	5.0	56.1	53.8	25.1	24	-
$PbTiO_3$	E_g	1.47	1.88	3.00	2.08	2.83	3.60
	V_0	60.4	70.4	65.2	64.9	62.4	62.6
	c/a	1.045	1.239	1.158	1.122	1.097	1.071
	P_s	0.80	1.26	1.14	1.06	1.03	~0.5 - 1.00
	ΔE	58.1	204.8	194.1	122.7	110.6	-
$BiFeO_3$	E_g	0.34	1.05 (1.76)	3.4	1.89	3.0	2.74
	V_0	345.1	382.7 (384.8)	375.1	369.8	369.0	373.9
	P_s	0.989	1.048 (1.003)	1.103	1.027	-	1.0
	μ	3.27	3.70 (3.95)	4.1	3.96	4.2	3.75

In the PBE column, the values of PBE with $U = 2$ correction are in parentheses. The B1WC hybrid GGA[37] designed for ferroelectric materials is used as the reference in the second last columns. E_g (eV) is the fundamental bandgap, V_0 (Å^3) is the volume, c/a is the ratio of the lattice constants c and a, and P_s (C m^{-2}) is the polarization of the tetragonal phases. ΔE (meV per cell) is the total energy difference between the cubic and tetragonal phases. $\mu(\mu_B)$ is the magnetic moment per Fe. The B1WC and experimental results for $BaTiO_3$ and $PbTiO_3$ are from ref. 37, and the hybrid GGAs and experimental results for $BiFeO_3$ are from ref. 38. The experimental polarization for $BiFeO_3$ is taken from ref. 52.

is often introduced for the LDA and PBE to account for the on-site Coulomb interaction and thus to open the bandgap. Table 2 shows that the SCAN bandgap is comparable to that of PBE+U with $U = 2$ eV for the Fe atoms[40]. Both SCAN and PBE+U give similar magnetic moments for Fe, as well as comparable polarizations. However, SCAN also yields more accurate predictions for the volume.

Limitations of semilocal functionals. The exchange-correlation hole is the density around an electron from which other electrons are excluded. Semilocal functionals must fail for systems where the exact exchange-correlation hole around an electron is quite delocalized, for example, the long-range van der Waals interaction and stretched H_2^+, where such functionals show a large self-interaction error. A long-range van der Waals correction has been applied to SCAN to further improve the descriptions for the van der Waals interaction (for example, the mean absolute relative error (MARE) of the binding energies of 28 layered materials is improved from about 60% for SCAN to 8%)[41]. Exact exchange mixing or self-interaction correction has to be applied to SCAN to better describe, for example, the hydrogen bonds between water molecules and reaction barriers.

Conclusions

We have demonstrated that accurate first-principles structures and energies of molecules and materials with diverse bonding are predicted by the non-empirical SCAN meta-GGA. These successes were unexpected from a computationally efficient functional. They suggest that a sufficiently sophisticated semilocal density functional can be broadly accurate, although not universally, and thus that the exact exchange-correlation hole around an electron is rather localized in many bonds at equilibrium. The examples unambiguously show that SCAN, without being fitted to any bonded system, accurately describes the major classes of molecular bonds, even better than the LDA or PBE GGA, which are of comparable efficiency. Furthermore, SCAN often yields an accuracy comparable to or better than hybrid GGAs. SCAN will therefore facilitate first-principles descriptions of systems with components dominated by different bonding characteristics, such as interfaces between different phases. Indeed, future work will show that SCAN has great predictive accuracy for the formation energies (and thus the relative stabilities) of solids and for phase transitions in liquids, which both require an accurate simultaneous description of different bonding types.

Methods

All our DFT calculations are self-consistent. Most of the *ab initio* calculations for the water monomer, dimer and hexamers were carried out in the Gaussian[42] code, except for those of PBE+vdW_TS and PBE0+vdW_TS, which were performed in FHI-aims[43]. The geometric, vibrational and electrostatic properties were calculated with the aug-cc-pvtz basis set in Gaussian and the tier-3 basis set in FHI-aims. The binding energies of the water dimer and hexamers were obtained by extrapolating to the complete basis set limit. The calculations for solids and liquids were performed using the VASP code and PAW potentials in the implementation of Kresse and Joubert[44]. For ice polymorphs, we used the geometries and computational settings of ref. 24. The phase-transition calculations for Si followed the settings of ref. 31. The interstitial defect calculations used an energy cutoff of 400 eV and a gamma-centred $4 \times 4 \times 4$ k-mesh. The defects were placed in and relaxed with the host atoms of a 64-atom simulation cell, with the lattice constant determined by the underlying functionals. AIMD simulations of liquid Si were performed with simulation cells of 216 atoms. An energy cutoff of 300 eV was used for the Si AIMD calculation. Production runs of 20 ps and the gamma-only k-mesh were used in all AIMD calculations and analysis. For simulations of ferroelectric and multiferroic materials, an energy cutoff of 600 eV was used. We used a tetragonal cell of five atoms and a gamma-centred $8 \times 8 \times 8$ k-mesh for $BaTiO_3$ and $PbTiO_3$, and a hexagonal cell of 30 atoms and a gamma-centred $4 \times 4 \times 2$ k-mesh for $BiFeO_3$. The spin configuration of $BiFeO_3$ was fixed to the G-type antiferromagnetic state. The spin–orbit coupling effect was neglected for all calculations. The spontaneous polarization was calculated according to the modern theory of polarization[45].

Received 15 November 2015; accepted 26 April 2016; published online 13 June 2016

References

1. Kohn, W. & Sham, L. J. Self-consistent equations including exchange and correlation effects. *Phys. Rev.* **140,** A1133–A1138 (1965).
2. Perdew, J. P. & Wang, Y. Accurate and simple analytic representation of the electron-gas correlation energy. *Phys. Rev. B* **45,** 13244–13249 (1992).
3. Sun, J., Perdew, J. P. & Seidl, M. Correlation energy of the uniform electron gas from an interpolation between high-and low-density limits. *Phys. Rev. B* **81,** 085123 (2010).
4. Perdew, J. P., Burke, K. & Ernzerhof, M. Generalized gradient approximation made simple. *Phys. Rev. Lett.* **77,** 3865–3868 (1996).
5. Perdew, J. P. *et al.* Restoring the density-gradient expansion for exchange in solids and surfaces. *Phys. Rev. Lett.* **100,** 136406 (2008).
6. Perdew, J. P., Burke, K. & Ernzerhof, M. Reply to the comment by Y. Zhang and W. Yang. *Phys. Rev. Lett.* **80,** 891 (1998).
7. Perdew, J. P., Ruzsinszky, A., Sun, J. & Burke, K. Gedanken densities and exact constraints in density functional theory. *J. Chem. Phys.* **140,** 18A533 (2014).
8. Sun, J., Perdew, J. P. & Ruzsinszky, A. Semilocal density functional obeying a strongly-tightened bound for exchange. *Proc. Natl Acad. Sci. USA* **112,** 685–689 (2015).
9. Becke, A. D. & Rousssel, M. R. Exchange holes in inhomogeneous systems: a coordinate-space model. *Phys. Rev. A* **39,** 3761–3767 (1989).
10. Tao, J., Perdew, J. P., Staroverov, V. N. & Scuseria, G. E. Climbing the density functional ladder: nonempirical meta-generalized gradient approximation designed for molecules and solids. *Phys. Rev. Lett.* **91,** 146401 (2003).

11. Zhao, Y. & Truhlar, D. G. A new local density functional for main-group thermochemistry, transition metal bonding, thermochemical kinetics, and noncovalent interactions. *J. Chem. Phys.* **125,** 194101 (2006).
12. Perdew, J. P., Ruzsinszky, A., Csonka, G. I., Constantin, L. A. & Sun, J. Workhorse semilocal density functional for condensed matter physics and quantum chemistry. *Phys. Rev. Lett.* **103,** 026403 (2009).
13. Sun, J., Xiao, B. & Ruzsinszky, A. Effect of the orbital-overlap dependence in the meta-generalized gradient approximation. *J. Chem. Phys.* **137,** 051101 (2012).
14. Del Campo, J. M., Gazquez, J. L., Trickey, S. B. & Vela, A. A new meta-GGA exchange functional based on an improved constraint-based GGA. *Chem. Phys. Lett.* **543,** 179–183 (2012).
15. Sun, J., Ruzsinszky, A. & Perdew, J. P. Strongly constrained and appropriately normed semilocal density functional. *Phys. Rev. Lett.* **115,** 036402 (2015).
16. Madsen, G. K. H., Ferrighi, L. & Hammer, B. Treatment of layered structures using a semilocal meta-GGA density functional. *J. Phys. Chem. Lett.* **1,** 515–519 (2010).
17. Becke, A. D. & Edgecombe, K. E. A simple measure of electron localization in atomic and molecular systems. *J. Chem. Phys.* **92,** 5397 (1990).
18. Silvi, B. & Savin, A. Classification of chemical bonds based on topological analysis of electron localization functions. *Nature* **371,** 683–686 (1994).
19. Sun, J. *et al.* Density functionals that recognize covalent, metallic, and weak bonds. *Phys. Rev. Lett.* **111,** 106401 (2013).
20. Perdew, J. P., Ernzerhof, M. & Burke, K. Rationale for mixing exact exchange with density functional approximations. *J. Chem. Phys.* **105,** 9982–9985 (1996).
21. Furche, F. & Perdew, J. P. The performance of semilocal and hybrid density functionals in 3*d* transition-metal chemistry. *J. Chem. Phys.* **124,** 044103 (2006).
22. Santra, B. *et al.* Hydrogen bonds and van der Waals forces in ice at ambient and high pressures. *Phys. Rev. Lett.* **107,** 185701 (2011).
23. Tkatchenko, A. & Scheffler, M. Accurate molecular van der Waals interactions from ground state electron density and free atom reference data. *Phys. Rev. Lett.* **102,** 073005 (2009).
24. Santra, B. *et al.* On the accuracy of van der Waals inclusive density-functional theory exchange-correlation functionals for ice at ambient and high pressures. *J. Chem. Phys.* **139,** 154702 (2013).
25. Santra, B. *et al.* On the accuracy of density-functional theory exchange-correlation functionals for H bonds in small water clusters: the water hexamer. *J. Chem. Phys.* **129,** 194111 (2008).
26. DiStasio, R. Jr, Santra, B., Li, Z., Wu, X. & Car, R. The individual and collective effects of exact exchange and dispersion interactions on the *ab initio* structure of liquid water. *J. Chem. Phys.* **141,** 084502 (2014).
27. Perdew, J. P. & Zunger, A. Self-interaction correction to density-functional approximations for many-electron systems. *Phys. Rev. B* **23,** 5048–5079 (1981).
28. Pederson, M. R., Ruzsinszky, A. & Perdew, J. P. Self-interaction correction with unitary invariance in density functional theory. *J. Chem. Phys.* **140,** 121103 (2014).
29. Hennig, R. G. *et al.* Phase transformation in Si from semiconducting diamond to metallic β-Sn phase in QMC and DFT under hydrostatic and anisotropic stress. *Phys. Rev. B* **82,** 014101 (2010).
30. Heyd, J., Scuseria, G. E. & Ernzerhof, M. Hybrid functionals based on a screened Coulomb potential. *J. Chem. Phys.* **118,** 8207–8215 (2003).
31. Xiao, B. *et al.* Testing density functionals for structural phase transitions of solids under pressure: Si, SiO_2 and Zr. *Phys. Rev. B* **88,** 184103 (2013).
32. Batista, E. R. *et al.* Comparison of screened hybrid density functional theory to diffusion Monte Carlo in calculations of total energies of silicon phases and defects. *Phys. Rev. B* **74,** 121102 (2006).
33. Sasaki, H., Tokizaki, E., Terashima, K. & Kimura, S. Density variation of molten silicon measured by an improved archimedian method. *Jpn J. Appl. Phys.* **33,** 3803–3807 (1994).
34. Waseda, Y. *et al.* High temperature X-ray diffraction study of melt structure of silicon. *Jpn J. Appl. Phys.* **34,** 4124–4128 (1995).
35. Cohen, R. E. Origin of ferroelectricity in perovskite oxides. *Nature* **358,** 136–138 (1992).
36. Kitchaev, D. A. *et al.* Energetics of MnO_2 polymorphs in density functional theory. *Phys. Rev. B* **93,** 045132 (2016).
37. Bilc, D. I. *et al.* Hybrid exchange-correlation functional for accurate prediction of the electronic and structural properties of ferroelectric oxides. *Phys. Rev. B* **77,** 165107 (2008).
38. Stroppa, A. & Picozzi, S. Hybrid functional study of proper and improper multiferroics. *Phys. Chem. Chem. Phys.* **12,** 5405–5416 (2010).
39. Wu, Z. & Cohen, R. E. More accurate generalized gradient approximation for solids. *Phys. Rev. B* **73,** 235116 (2006).
40. Neaton, J. B., Ederer, C., Waghmare, U. V., Spaldin, N. A. & Rabe, K. M. First-principles study of spontaneous polarization in multiferroic $BiFeO_3$. *Phys. Rev. B* **71,** 014113 (2005).
41. Peng, H., Yang, Z., Sun, J. & Perdew, J. P. SCAN+rVV10: a promising van der Waals density functional. Preprint at https://arxiv.org/abs/1510.05712 (2015).
42. Frisch, M. J. *et al. Gaussian 03 Revision D.02* (Gaussian, 2004).
43. Blum, V. *et al. Ab initio* molecular simulations with numeric atom-centered orbitals. *Comp. Phys. Comm.* **180,** 2175–2196 (2009).
44. Kresse, G. & Joubert, D. From ultrasoft pseudopotentials to the projector augmented-wave method. *Phys. Rev. B* **59,** 1758–1775 (1999).
45. King-Smith, R. D. & Vanderbilt, D. Theory of polarization of crystalline solids. *Phys. Rev. B* **47,** 1651–1654 (1999).
46. Brandenburg, J. G., Maas, T. & Grimme, S. Benchmarking DFT and semiempirical methods on structures and lattice energies for ten ice polymorphs. *J. Chem. Phys.* **142,** 124104 (2015).
47. Whalley, E. Energies of the phases of ice at zero temperature and pressure. *J. Chem. Phys.* **81,** 4087–4092 (1984).
48. Xu, X. & Goddard, III, W. A. Bonding properties of the water dimer: a comparative study of density functional theories. *J. Phys. Chem. A* **108,** 2305–2313 (2004).
49. Shank, A. *et al.* Accurate *ab initio* and 'hybrid' potential energy surfaces, intramolecular vibrational energies, and classical IR spectrum of the water dimer. *J. Chem. Phys.* **130,** 144314 (2009).
50. Rocher-Casterline, B. E., Ch'ng, L. C., Mollner, A. K. & Reisler, H. Determination of the bond dissociation energy (D_0) of the water dimer, $(H_2O)_2$, by velocity map imaging. *J. Chem. Phys.* **134,** 211101 (2011).
51. Salek, P. *et al.* A comparison of density-functional-theory and coupled-cluster frequency-dependent polarizabilities and hyperpolarizabilities. *Mol. Phys.* **103,** 439–450 (2005).
52. Lebeugle, D., Colson, D., Forget, A. & Viret, M. Very large spontaneous electric polarization in $BiFeO_3$ single crystals at room temperature and its evolution under cycling fields. *Appl. Phys. Lett.* **91,** 022907 (2007).

Acknowledgements

This research was supported as part of the Center for the Computational Design of Functional Layered Materials, an Energy Frontier Research Center funded by the US Department of Energy (DOE), Office of Science, Basic Energy Sciences (BES), under award no. DE-SC0012575. Computer equipment in Temple's HPC Center was supported by the National Science Foundation (NSF) under major research instrumentation grant no. CNS-09-58854. J.S., R.C.R., Y.Z., Z.S., A.R. and H.P. acknowledge support in the form of computer time from the National Energy Research Scientific Computing Center (NERSC), a DOE Office of Science User Facility, and the HPC Center of Temple University. X.W. and Y.Z. acknowledge support from the American Chemical Society Petroleum Research Fund (ACS PRF) under grant no. 53482-DNI6. J.S., A.R., X.W. and J.P.P. thank R. Car, G.I. Csonka, B. Santra and R. DiStasio Jr for discussions. This article is dedicated to the memory of Walter Kohn.

Author contributions

J.S. and J.P.P. designed the project. J.S., R.C.R., Y.Z., Z.S., A.R. and H.P. carried out the calculations. J.S. implemented the SCAN metaGGA and prepared the initial manuscript. All authors contributed to the discussions and revisions of the manuscript.

Additional information

Supplementary information is available in the online version of the paper. Reprints and permissions information is available online at www.nature.com/reprints. Correspondence and requests for materials should be addressed to J.S.

Competing financial interests

The authors declare no competing financial interests.